Geophysical Journal International

Geophys. J. Int. (2019) **216,** 777–793
Advance Access publication 2018 November 3
GJI Geodynamics and tectonics

doi: 10.1093/gji/ggy465

Inertial modes in near-spherical geometries

J. Rekier, A. Trinh, S.A. Triana and V. Dehant

Royal Observatory of Belgium, E-mail: jeremy.rekier@observatory.be

Accepted 2018 November 2. Received 2018 October 29; in original form 2018 April 05

SUMMARY

We propose a numerical method to compute the inertial modes of a container with near-spherical geometry based on the fully spectral discretization of the angular and radial directions using spherical harmonics and Gegenbauer polynomial expansion, respectively. This allows to solve simultaneously the Poincaré equation and the no penetration condition as an algebraic polynomial eigenvalue problem. The inertial modes of an exact oblate spheroid are recovered to machine precision using an appropriate set of spheroidal coordinates. We show how other boundaries that deviate slightly from a sphere can be accommodated for with the technique of *equivalent spherical boundary* and we demonstrate the convergence properties of this approach for the triaxial ellipsoid.

Key words: Core; Numerical solutions; Planetary interiors.

1 INTRODUCTION

Coriolis forces in a rotating fluid support oscillatory motions known as inertial waves. When the fluid is rotating inside a boundary, as is the case for many astrophysical objects including our planet, inertial *modes* can exist. Experimentally, these modes can be excited mechanically by means of libration of the bounding surface (Aldridge & Toomre 1969), by precession (Malkus 1968), by tidal forces (Morize *et al.* 2010) or by the differential rotation of a solid inner core (Kelley *et al.* 2007). Although the first theoretical studies of inertial modes date back towards the end of the 19th century, with the works of Thomson (1880), Poincaré (1885) and Bryan (1889), the role of inertial modes in the dynamics of rotating stars, planets and other astrophysical bodies remains largely unexplored.

With an eye towards the dynamics of bodies deformed by rotation and tides, it is relevant to obtain the solutions for inertial mode oscillations of rotating fluids within *near-spherical* boundaries such as spheroids or triaxial ellipsoids. In the analytical realm, implicit solutions for inviscid inertial eigenmodes in a spheroid were first obtained by Bryan (1889) using bi-spheroidal coordinates. In a triaxial ellipsoid the first relevant work is that of Hough (1895), who employed Lamé functions. Explicit solutions in the spheroid for few low-degree modes were obtained much later by Kudlick (1966). Explicit solutions for all inertial eigenmodes in a spheroid were not available until the relatively recent work of Zhang *et al.* (2004), who also included the first-order viscous corrections. In the case of a triaxial ellipsoid, Vantieghem (2014) provided an algorithm to construct analytical inviscid solutions that are linear and quadratic in the Cartesian coordinates, with the possibility to include higher order solutions. The long standing question about the completeness of the inertial modes to represent any smooth fluid flow within a full rotating ellipsoid was answered affirmatively by the work of Backus & Rieutord (2017) and Ivers (2017a). It turns out that inertial modes are also complete when the rotation axis is arbitrary with respect to the principal axes of the ellipsoid (Ivers 2017b).

In the numerical realm, studies of inertial eigenmodes in ellipsoids are based predominantly on finite element methods (e.g. Cébron *et al.* 2010; Chan *et al.* 2010; Vantieghem 2014). The works of Schmitt (2006) and Schmitt & Jault (2004) are perhaps the only ones using a set of oblate spheroidal coordinates. All these numerical studies usually focus on the time evolution of the flow field inside the spinning ellipsoid, which is in turn subject to some kind of additional mechanical forcing (e.g. libration) to excite inertial modes.

The purpose of this paper is the numerical computation of the inertial modes of a fluid rotating inside an ellipsoidal boundary numerically using a fully spectral discretization. The radial direction is discretized using a relatively recent technique that employs Chebyshev and Gegenbauer polynomials (Olver & Townsend 2013). This has the advantage to result in a sparse matrix representation of differential operators. The discretization in the angular directions is carried out using a spherical harmonics decomposition. For the special cases of an exactly spherical or oblate spheroidal container, the spectral decomposition can be used to recover the inertial modes with an accuracy that is limited only by numerical precision. In order to treat the triaxial case, we extend the equivalent spherical domain technique introduced by Smith (1974) and substantiate it with an analysis of numerical convergence. This makes it possible, at least in principle, to compute the inertial modes for any boundary that deviates only slightly from sphericity. We also demonstrate a technique to recover semi-analytical solutions in

an oblate spheroid and in a triaxial ellipsoid using systems of bi-spheroidal and bi-ellipsoidal coordinates. This allows us to cross-validate both approaches.

Our numerical method paves the way for future extensions of the model to accommodate features that the analytical solutions are not capable of, such as the inclusion of viscosity, magnetic effects or stratification and, most prominently, the effect of boundary topography.

The inviscid problem that we present in this study is an interesting instance of a *polynomial eigenvalue problem* with a non-standard boundary condition. This problem also serves as a concrete example demonstrating the potential of a more general method that we have developed to treat similar problems consisting of general systems of *Partial Differential Equations* (PDEs) in *near-spherical geometries*.

The paper is structured as follows. In Section 2, we review the mathematical description of inertial waves inside a cavity before we explain the methods used to solve the resulting equations numerically. In Section 3, we demonstrate the validity of our approach by treating the case of a flow within an ellipsoidal boundary. Section 4 provides a discussion of how the method can easily be extended to more complex systems. Appendix at the end of this paper provides details on how to compute the analytical solutions to the inertial modes as well as other useful technical information used throughout this paper.

2 METHOD

2.1 Mathematical description of inertial modes

We consider an incompressible, homogeneous and inviscid fluid contained in a rigid cavity which rotates with angular velocity, Ω around the z-axis, $\hat{\mathbf{z}}$. In the frame attached rigidly to the rotating cavity and using $1/\Omega$ as the unit of time, the momentum balance reads

$$\partial_t \mathbf{u} + 2\hat{\mathbf{z}} \times \mathbf{u} = -\nabla p, \tag{1}$$

where $\mathbf{u}$ represents the flow velocity and p the reduced pressure (which includes the centrifugal and gravitational potential). We are assuming that the fluid velocity is small compared to the maximum tangential velocity of the cavity so that we can discard the nonlinear $(\mathbf{u} \cdot \nabla)\mathbf{u}$ term. We further assume that the fluid motion is periodic in time:

$$\mathbf{u} = \mathbf{u}_0(\mathbf{r})\mathrm{e}^{2\mathrm{i}\lambda t} + \mathbf{u}_0^*(\mathbf{r})\mathrm{e}^{-2\mathrm{i}\lambda t}, \tag{2}$$

$$p = p_0(\mathbf{r})\mathrm{e}^{2\mathrm{i}\lambda t} + p_0^*(\mathbf{r})\mathrm{e}^{-2\mathrm{i}\lambda t}, \tag{3}$$

where $*$ denotes the complex conjugate. After some algebraic manipulation, eq. (1) reduces to the so-called Poincaré equation for the pressure amplitude p_0 (Poincaré 1885):

$$-\lambda^2 \nabla^2 p_0 + (\hat{\mathbf{z}} \cdot \nabla)^2 p_0 = 0, \tag{4}$$

where λ is the half-frequency of the motion. We employ a no-penetration boundary condition for the velocity $\mathbf{u} \cdot \hat{\mathbf{n}}|_{\partial\mathcal{V}} = 0$ at the bounding surface $\partial\mathcal{V}$, which translates into the following condition for the pressure field p_0 (Greenspan 1968):

$$-\lambda^2 \hat{\mathbf{n}} \cdot \nabla p_0 + \mathrm{i}\lambda(\hat{\mathbf{z}} \times \hat{\mathbf{n}}) \cdot \nabla p_0 + (\hat{\mathbf{n}} \cdot \hat{\mathbf{z}})(\hat{\mathbf{z}} \cdot \nabla p_0)|_{\partial\mathcal{V}} = 0. \tag{5}$$

The velocity field can be recovered from the solution for p using the following expression:

$$\mathbf{u}_0 \equiv \frac{1}{1-\lambda^2}\frac{1}{2}\left(\hat{\mathbf{z}} \times \nabla p_0 - \mathrm{i}\lambda \nabla p_0 + \frac{\mathrm{i}}{\lambda}(\hat{\mathbf{z}} \cdot \nabla p_0)\hat{\mathbf{z}}\right). \tag{6}$$

Finding analytical solutions to the problem just described proceeds in two steps. The first one is a change of coordinates that reduces eq. (4) to a Laplace equation. The Laplace operator and the boundary condition both must be separable in these coordinates, something that is only possible in a limited number of coordinates. The second step is to inject the formal solution of the Laplace equation into the boundary condition and solve for λ. We give a detailed illustration for the cases of the sphere, the oblate spheroid and the triaxial ellipsoid in Appendix A. The solutions obtained will serve us to validate the numerical results of Section 3.

The system of eqs (4) and (5) can be cast numerically as an eigenvalue problem that is *polynomial in the eigenvalue* λ. There are methods to solve algebraic systems of this type. In order to use these, we first turn the above differential problem into an algebraic problem of the form

$$(A_0\lambda^0 + A_1\lambda^1 + A_2\lambda^2)\mathbf{x} = 0, \tag{7}$$

where the A_i's are square matrices, Fig. 1 gives a visual representation of these matrices. Section 2.2 explains how these can be obtained from eqs (4) and (5).

The direct numerical resolution of the Poincaré equation for the motion of a rotating fluid is not very common practice. The reason being that this formulation is not valid when viscosity is taken into account. When this is the case, one uses an approach based on the following decomposition of the (solenoidal) velocity field, $\boldsymbol{u}$:

$$\boldsymbol{u} = \boldsymbol{\nabla} \times \boldsymbol{\nabla} \times (P\boldsymbol{r}) + \boldsymbol{\nabla} \times (T\boldsymbol{r}), \tag{8}$$

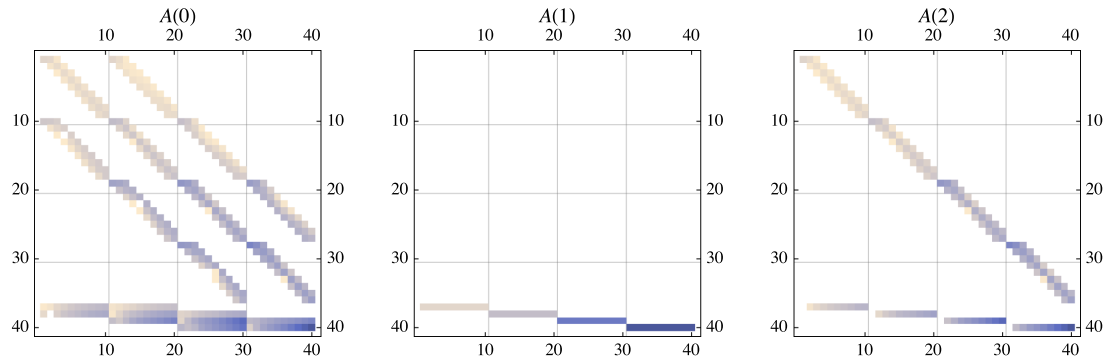

(A) Sphere (spherical coordinates)

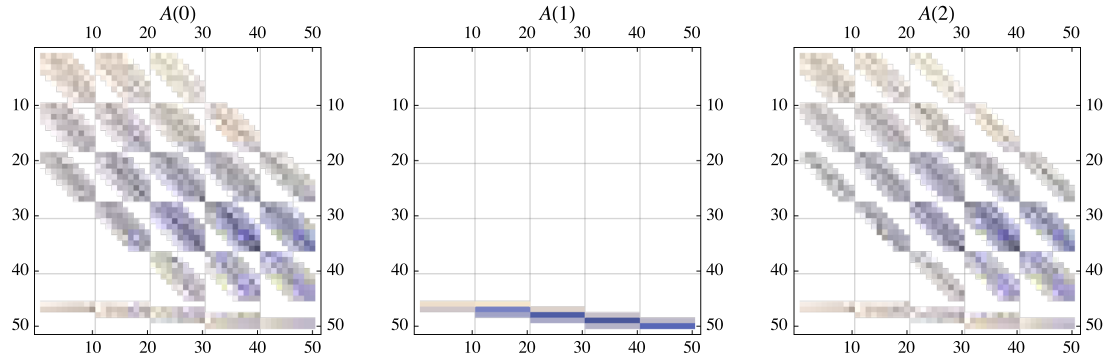

(B) Spheroid (oblate spheroidal coordinates)

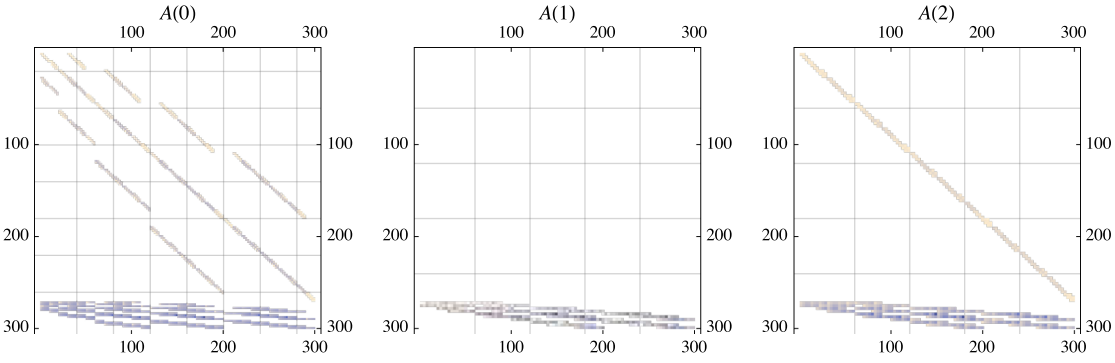

(C) Triaxial ellipsoid (spherical coordinates with series expansion of b.c.)

Figure 1. Matrix representation of the Poincaré system eqs (4) and (5) for three types of boundary. The rows dedicated to boundary conditions can be seen at the bottom of each matrix ($N = 20$, $L = 10$).

where $P(\boldsymbol{r})$ and $T(\boldsymbol{r})$ are the *poloidal* and *toroidal* scalar fields, respectively. After inserting the above in the momentum eq. (1), one can write two independent scalar equations for P and T by separately considering the radial projections of the curl of the momentum equation and the curl of its curl (Rieutord & Valdettaro 1997). This latter approach can be used as well when dealing with the inviscid problem so long as the domain of integration encloses the origin of coordinates, that is, containers that share the topology of the spherical shell are prohibited (Rieutord *et al.* 2000).

Both methods have their own advantages and drawbacks. The formulation in P and T, when discretized, leads to a linear eigenvalue problem and so allows the usage of state of the art codes designed for viscous computations with minor modifications. On the other hand the formulation in p leads to a quadratic eigenvalue problem but the scalar nature of the Poincaré equation makes it straightforwardly adaptable to oblate spheroidal coordinates as discussed in Appendix C.

In the rest of this section, we give the details of the discretization method assuming the formulation in terms of the Poincaré equation. Both formulations are used to obtain the results of Section 3.

2.2 Spectral discretization

2.2.1 Angular discretization

When working in spherical coordinates $\{r, \theta, \phi\}$, the PDE (4) can be reduced to a set of coupled *Ordinary Differential Equations* (ODEs) using the method of spherical harmonics decomposition. The pressure field amplitude p_0 is written as the following truncated series:

$$p_0(r, \theta, \phi) = \sum_{\ell=0}^{L} \sum_{m=-\ell}^{\ell} p_{\ell,m}(r) Y_\ell^m(\theta, \phi), \tag{9}$$

where L is an integer chosen as large as possible. The numerical task consists in finding an approximate expression for the radial functions $\{p_{\ell,m}(r)\}$. In the end, the resulting system will be turned into a fully algebraic (matrix) problem by discretization of the radial direction.

We now review symmetry considerations which allow to decouple the problem further. The second term of eq. (4) induces a coupling between each harmonic component (ℓ, m) and its closest neighbours with a degree of the same parity $(\ell \pm 2, m)$. The origin of the coupling traces back to the presence of the Coriolis force in the momentum equation. Appendix B gives the analytical expression of this term as well as the last two terms of eq. (5) in spherical coordinates illustrating the case of a spherical container ($\hat{\mathbf{n}} = \hat{\mathbf{r}}$). The boundary condition induces no further coupling of the spherical harmonics components in that case. Moreover, components with different azimuthal m numbers remain uncoupled, an important fact that is carried over to the spheroidal container case (or indeed any axisymmetric container) and allows to solve for modes with different m independently. This classification of modes by their azimuthal m number is no longer applicable for (non-axisymmetric) ellipsoidal containers.

The nature of the coupling of the ℓ-numbers reflects the decoupling of modes with a pressure profile that is symmetric by reflection across the equatorial plane and those that are antisymmetric. By using the property, $Y_\ell^m(\theta, \phi) = (-1)^{\ell+m} Y_\ell^m(\pi - \theta, \phi)$, one can show that modes with $(\ell + m)$ **even** are symmetric modes while those with $(\ell + m)$ **odd** are antisymmetric modes.

Following the above considerations, the layout of the radial functions $p_{\ell,m}(r)$ (which will become the eigenvectors) prior to their discretization in r reads

$$\left\{p_{|m|,m}, p_{|m+2|,m}, p_{|m+4|,m}, \dots\right\}^{\mathrm{T}} \quad \text{for equatorially sym. modes,} \tag{10a}$$

$$\left\{p_{|m+1|,m}, p_{|m+3|,m}, p_{|m+5|,m}, \dots\right\}^{\mathrm{T}} \quad \text{for equatorially antisym. modes.} \tag{10b}$$

2.2.2 Radial discretization

For the radial discretization we follow the method proposed by Olver & Townsend (2013) based on polynomial expansion on the (truncated) basis of Chebyshev polynomials for the radial functions and Gegenbauer polynomials for their radial derivatives. Its main advantage compared to the more common collocation methods is that the matrices that result from the discretization of differential operators are small in size and *sparse*, as opposed to the collocation methods that lead to small but *dense* matrices for equal resolution. Finite difference methods lead to large sparse matrices and do not provide exponential convergence. The sparsity of the resulting matrices in the method of Olver & Townsend (2013) is particularly handy if very high numerical resolution is needed. The only drawback is that it is slightly less straightforward to implement. The use of Chebyshev polynomials is especially convenient due to the possibility to compute coefficients using a *fast Fourier transform*.

We deal with bounding surfaces that deviate slightly from sphericity, with R representing the mean radius of the cavity. In its original form, the spectral method of Olver & Townsend (2013) is designed to deal with differential equations in a single spatial direction x, limited to the interval $x \in [-1, 1]$. Special care is needed when we consider the radial domain $[0, R]$ of the fluid. One might naively map the radial fluid domain $[0, R]$ to the $[-1, 1]$ interval and enforce the appropriate boundary condition (the regularity condition at the centre of coordinates) at $x = -1$. This is however a poor choice because the resulting radial functions are not necessarily compatible with the intrinsic symmetries of the spherical harmonics. A better choice is to extend the fluid domain to $[-R, R]$ and map it to the interval $[-1, 1]$ to match the natural domain of the Chebyshev polynomials. Since the spherical harmonics satisfy

$$Y_\ell^m(\theta + \pi, \phi) = (-1)^\ell Y_\ell^m(\theta, \phi), \tag{11}$$

the following identity holds for the pressure field $p_0(\mathbf{r})$:

$$p_0(-r, \theta, \phi) = p_0(r, \pi - \theta, \phi + \pi), \tag{12}$$

which implies

$$p_{\ell,m}(-r) = (-1)^\ell p_{\ell,m}(r). \tag{13}$$

In our approach each function $p_{\ell,m}(r)$ will be represented as a linear combination of Chebyshev polynomials, $T_k(x)$: $p_{\ell,m}(r) = \sum_{k=0}^{N} p_{\ell,m}^k T_k(r/R)$. As the parity of each Chebyshev polynomial can be read from that of its integer index, k, the condition eq. (13) can be enforced by only keeping the coefficients $p_{\ell,m}^k$ that have the correct parity.

Boundary conditions are enforced by row replacement (Olver & Townsend 2013) after expansion on spherical harmonics.

One important detail that we need to point out is the fact that, when treating a given problem, one should always try to eliminate inverse powers of r from the starting expression. This in order to keep the Chebyshev expansion of any pre-factor in the equation as small as possible which greatly reduces the bandwidth of every block matrix (Olver & Townsend 2013). For example, the first step in dealing with eq. (4) is to multiply it by r^2.

The usage of spherical harmonics can be extended to equations written in oblate spheroidal coordinates. An explanation of how to do this is given in Appendix C.

Fig. 1(a) shows an example of the final set of matrices making up the discretized version of eqs (4) and (5) for a spherical container using spherical coordinates. The rows dedicated to the enforcement of the boundary condition can be seen at the bottom of each matrix. Fig. 1(b) shows the same set of matrices for a spheroidal container using the oblate spheroidal coordinates. Note that the number of blocks is larger compared to the spherical case of Fig. 1(a). This illustrates the more extensive coupling between the spherical harmonics components $p_{\ell,m}$. Each individual block also has a wider diagonal representing the increased number of coefficients needed in the polynomial expansion of each component.

2.3 Near-spherical boundaries

When dealing with non-spherical domains, the use of spherical harmonic decomposition must be adapted. We now present a general way to do so. In essence, it amounts to treat the position of the physical boundary as the result of a series expansion around the sphere. For this reason, this method is only efficient when dealing with *near-spherical boundaries*. The radius of the physical boundary becomes a function of θ and ϕ which we parametrize as

$$\begin{aligned} R(\theta,\phi) &= R_0\,(1+\epsilon(\theta,\phi)) \\ &= R_0\left(1+\sum_{\ell=0}^{\infty}\sum_{m=-\ell}^{\ell}\epsilon_{\ell,m}Y_\ell^m(\theta,\phi)\right). \end{aligned} \tag{14}$$

The technique will work better if $\varepsilon(\theta,\phi) \ll 1$ and the coefficients $\varepsilon_{\ell,m}$ are small. The trick is to transform a boundary condition at $r = R(\theta,\phi)$, the *physical boundary*, into a condition on an equivalent spherical domain, the *computational boundary* (Smith 1974). For example, suppose that one wishes to impose the Dirichlet boundary condition on a single scalar field $\zeta(r,\theta,\phi)$. At the physical boundary, the condition is simply $\zeta|_R = 0$. Assuming a small deviation from the spherical boundary, one can write

$$\zeta|_R = \zeta|_{R_0} + \frac{\mathrm{d}\zeta}{\mathrm{d}r}|_{R_0}(R-R_0) + \mathcal{O}(\epsilon^2) = 0. \tag{15}$$

Using eq. (14), one finds the following expansion in spherical harmonics:

$$\sum_{\ell=0}^{L}\sum_{m=-\ell}^{\ell}\left(\zeta_{\ell,m}|_{R_0}Y_\ell^m + \sum_{\ell'=0}^{L}\sum_{m'=-\ell'}^{\ell'}\frac{\mathrm{d}\zeta_{\ell,m}}{\mathrm{d}r}|_{R_0}\epsilon_{\ell',m'}Y_\ell^m Y_{\ell'}^{m'}\right) + \mathcal{O}(\epsilon^2) = 0. \tag{16}$$

The product of spherical harmonics can then be reduced to a sum using *3-j symbols*. which will generally consist of $2\ell' + 1$ terms featuring spherical harmonics ranging from $Y^m_{|\ell-\ell'|}$ to $Y^m_{\ell+\ell'}$. Those terms effectively couple together these harmonics with Y_ℓ^m from the original expression. Imposing the Dirichlet boundary condition—in its series expansion form—is therefore equivalent to equating each spherical harmonics component of eq. (16) to zero independently. It is possible to increase the precision of this scheme by keeping higher powers of ε in the Taylor expansion eq. (15). This will bring out products of spherical harmonics that include more factors resulting in more extensive coupling in the spherical harmonics.

In general, the expression of the boundary condition may also contain vectors. It is actually the case for eq. (5) which features the pressure gradient, $\boldsymbol{\nabla} p$, and the normal vector $\hat{\mathbf{n}}$. In such cases, the procedure is similar to what we have described, except that we now have to expand both $\hat{\mathbf{n}}$ and $\boldsymbol{\nabla} p$ onto a basis of vector spherical harmonics. The idea remains the same although the handling of symbolic expressions can become quite tedious. In practice, we use *TenGSHui*, a dedicated Mathematica package (Trinh, in preparation), for these manipulations.

The technique described above can be used to deal with ellipsoidal boundaries with small eccentricities. Such boundaries can be parametrized as

$$x^2 + \frac{y^2}{(1-f^2)} + \frac{z^2}{(1-e^2)} = a^2, \tag{17}$$

where a^2 stands for the semi-major axis of the ellipsoid in the equatorial plane and e^2 and f^2 (both taken as $\ll 1$), respectively represent the polar and equatorial squared eccentricities in the principal axes of symmetry of the ellipsoid.

We have already argued that the spherical harmonics components with different azimuthal m numbers decouple in the special case when $f^2 = 0$ (see Section 2.2.1). In the general (triaxial) case, the spherical harmonics expansion will contain terms with different m numbers. The extra amount of coupling greatly increases the computational cost when one increases the angular resolution, that is, the upper bound on the ℓ number (see eq. 9). The considerations on the decoupling of the equatorially symmetric and antisymmetric modes, however remains valid

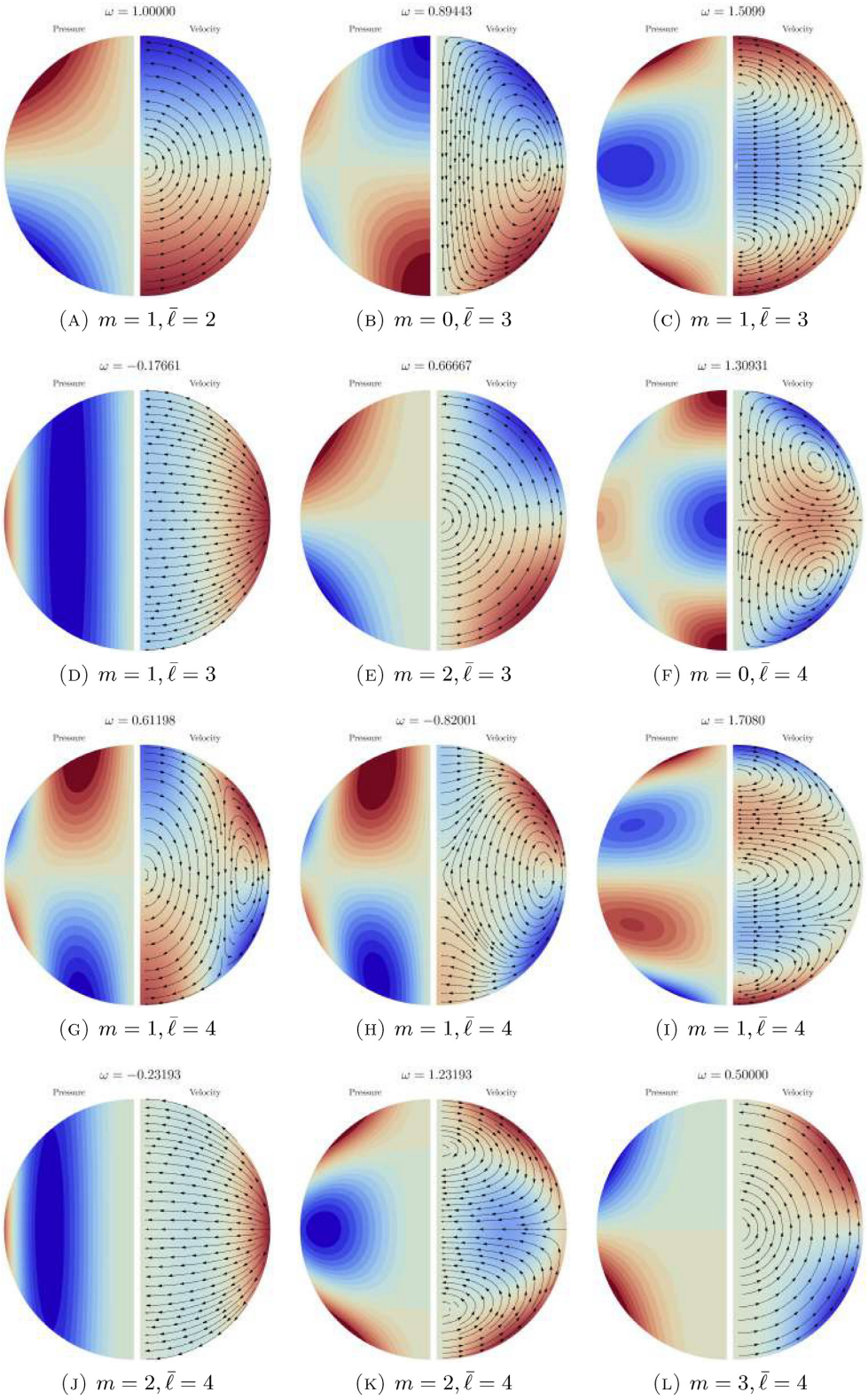

Figure 2. Numerical solutions of inviscid inertial modes in a sphere. On each figure, the colours represent the azimuthal component of the velocity on the right and the intensity of the (reduced) pressure inside the cavity on the left. Red corresponds to positive values, blue to negative values. The plots of pressure field are inverted images of the region on the right of each plot. ($N = 20$, $L = 10$).

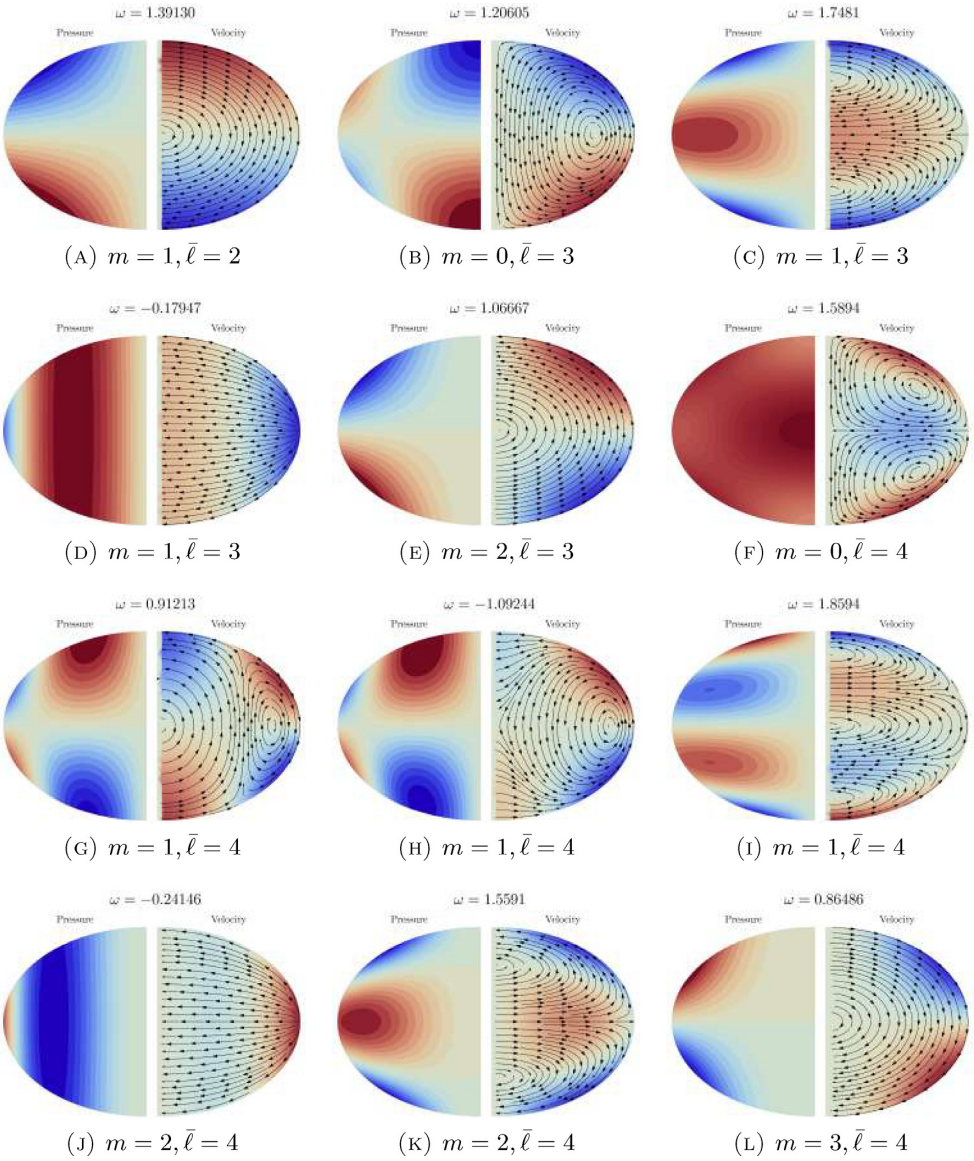

Figure 3. Similar to Fig. 2 but for an oblate spheroid with squared eccentricity $e^2 = \frac{9}{16}$. ($N = 40$, $L = 20$).

with the effect that the shape function, $\varepsilon_{\ell,m}$, (see eq. 14) contains only even ℓ and m numbers.[1] This ensures that modes with even m in an axisymmetric container will have a triaxial counterpart whose expansion contains only even m numbers. The same is true of axisymmetric modes with an odd m number. Fig. 1(c) shows the matrices involved in the discretized versions of eqs (4) and (5) for a triaxial ellipsoid using the method of series expansion of the boundary condition. Note the larger size of the matrices compared to Figs 1(a) and (b) due to the extra coupling between the coefficients with different m numbers in the boundary conditions.

2.4 Solver

We solve the algebraic problem resulting from the discretization of eqs (4) and (5) using the SLEPc package (Hernandez *et al.* 2005). SLEPc is an open-source software built on top of PETSc, another open-source package dedicated to efficiently solve large matrix equations (Balay *et al.* 1997, 2017a,b). SLEPc is the part that deals with eigenvalue problems. As the matrices involved in our problem can be quite large, it is impractical to solve for the whole eigenspectrum. Instead, we perform a *shift-and-invert* spectral transformation of the original problem that greatly improves the efficiency by limiting the computation of the spectrum to a small region around a given target eigenvalue (the pivot) provided as a guess by the user. Our own usage of SLEPc was greatly inspired by the one described by Vidal & Schaeffer (2015). The only

[1] the explicit expression of each coefficient $\varepsilon_{\ell,m}$ is given in Appendix D.

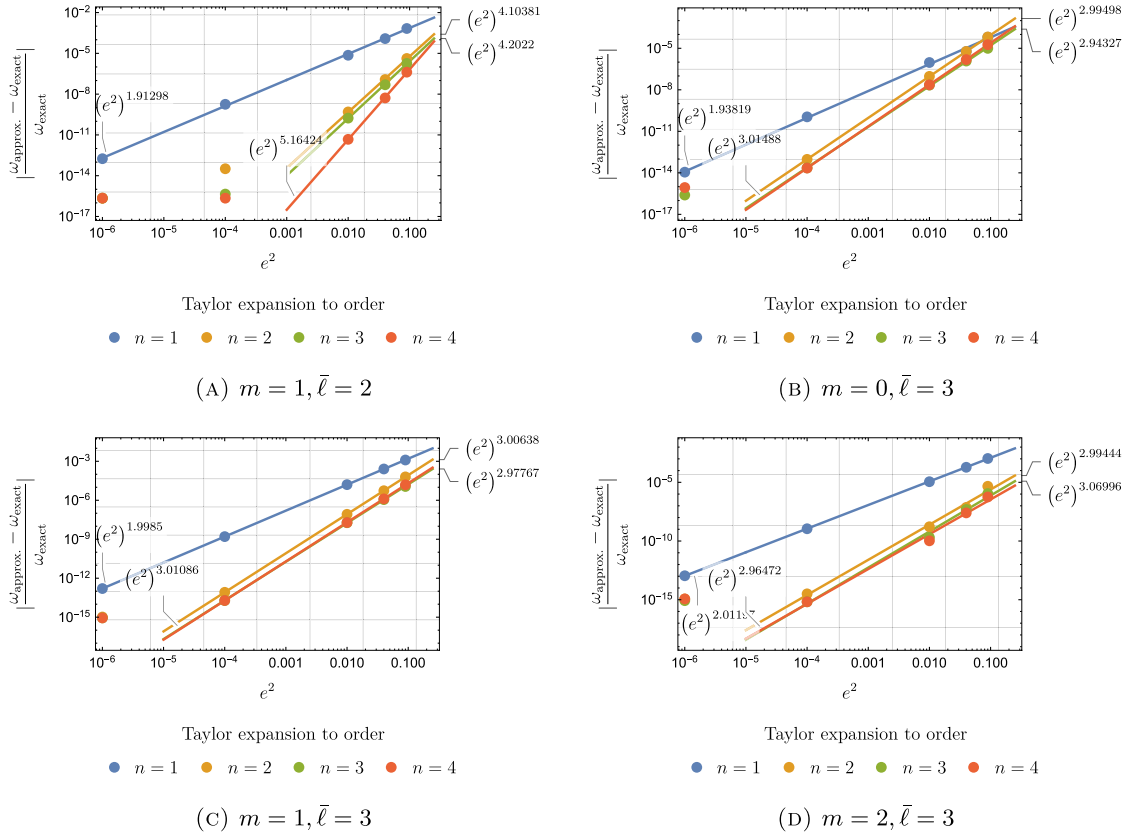

(A) $m = 1, \bar{\ell} = 2$ (B) $m = 0, \bar{\ell} = 3$

(C) $m = 1, \bar{\ell} = 3$ (D) $m = 2, \bar{\ell} = 3$

Figure 4. Oblate spheroid—comparison of the eigenvalue of the first inertial modes computed using a Taylor expansion of the boundary condition with their analytical values as a function of the squared eccentricity e^2 ($N = 20$, $L = 10$).

difference being that we make use of the built-in PEP solver (Campos & Roman 2016). The shift and invert method was also used by Rieutord & Valdettaro (1997) in a similar context.

3 RESULTS

We apply the methods of the previous section to the computation of the inertial modes in an ellipsoid. We start with the spherical case before considering the oblate spheroid and finally the triaxial ellipsoid.

3.1 Sphere

Fig. 2 shows meridional cuts in the spatial velocity profiles of the first 12 inertial modes in order of increasing spatial complexity. Each mode is identified by its (single) azimuthal m number, its maximum ℓ number, $\bar{\ell}$, and its physical frequency, $\omega = 2\lambda$. The first of these modes which corresponds to $\bar{\ell} = 2$ and $m = 1$ is of particular importance and is called the *spin-over mode*. In the rotating reference frame, this mode corresponds to a solid body rotation around an axis, itself rotating within the equatorial plane with unit angular frequency. The computation was carried out using a set of Chebyshev polynomials with maximum degree $N = 20$ and a maximum degree of spherical harmonics $L = 10$. The values of the frequencies that we compute agree with the analytical predictions of eq. (A16) to numerical precision.

3.2 Oblate spheroid

Fig. 3 is analogous to Fig. 2 for a spheroidal container of squared eccentricity $e^2 = \frac{9}{16}$. The resolution used is $N = 20$, $L = 10$. The values of the eigenfrequencies again agree with the analytical prediction of eq. (A16) to numerical precision.

These results were computed using the specially tailored set of oblate spheroidal coordinates (Appendix C).

The inertial modes of an oblate spheroid can also be computed using the technique of equivalent spherical boundary exposed in Section 2.3. Fig. 4 shows the difference between the numerical and analytical eigenvalues for the inertial modes of lowest maximum degree, $\bar{\ell}$. The integer, n, represents the maximum order of the Taylor expansion. The error made on the computed eigenfrequencies scales as some near-integer power of the squared eccentricity. We see that the precision on the numerical eigenvalues saturates to second order convergence for all modes except the spin-over ($\bar{\ell} = 2, m = 1$). We attribute this to the fact of working in finite arithmetic precision. The simple geometry

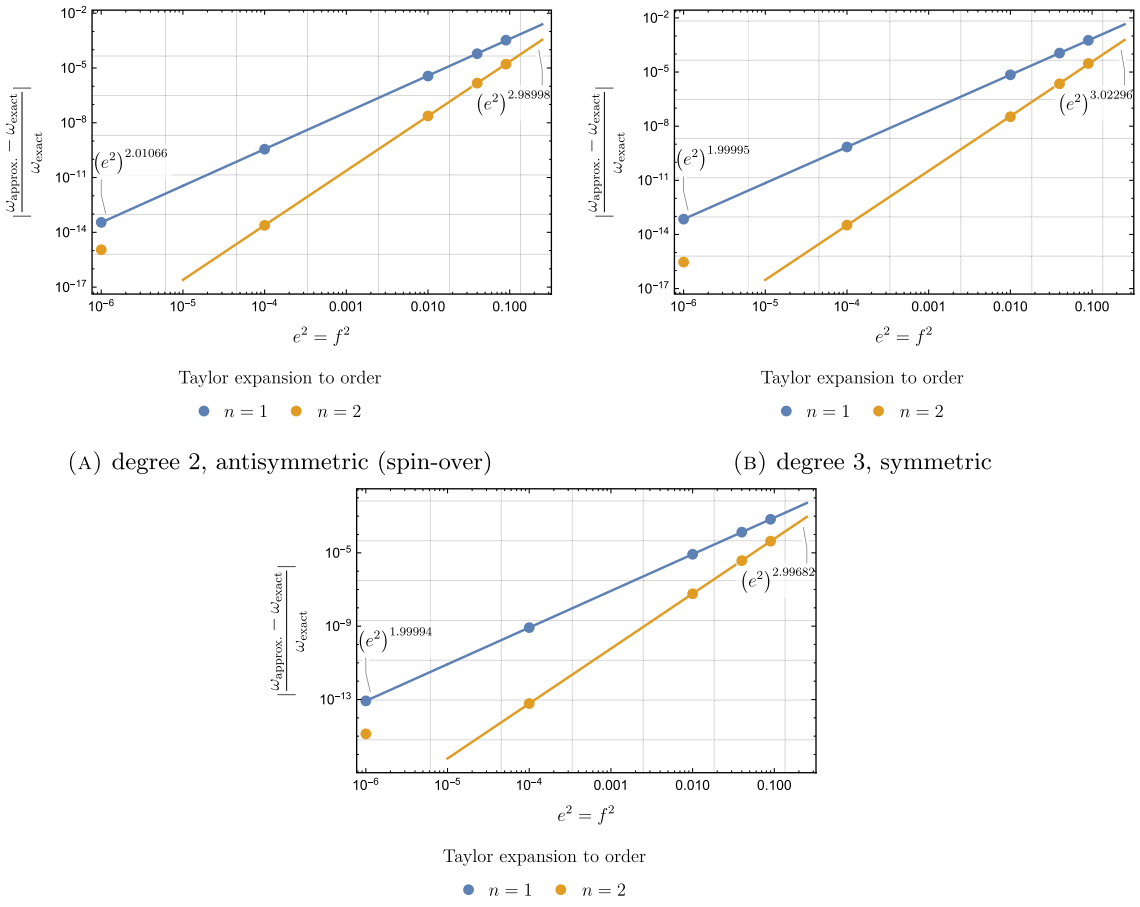

(A) degree 2, antisymmetric (spin-over)

(B) degree 3, symmetric

(C) degree 3, antisymmetric

Figure 5. Triaxial ellipsoid—comparison of the eigenvalue of three inertial modes computed using a Taylor expansion of the boundary condition with their analytical values as a function of the squared eccentricities $e^2 = f^2$ ($N = 20$, $L = 12$).

of the spin-over mode somehow makes this issue less important. Interestingly, the error for $n = 2$ for this mode already scales as $\sim(e^2)^4$ so that nothing is gained by using $n = 3$.

3.3 Triaxial ellipsoid

The Taylor expansion of the boundary condition is performed in the two eccentricity parameters e^2 and f^2, which are considered of the same order of magnitude. Fig. 5 shows the residual error on three eigenvalues in the special case where $e^2 = f^2$. The error scales as expected for Taylor expansion to order $n = 1$ and $n = 2$, respectively.

Fig. 6(a) shows the error on the evaluation of the spin-over frequency as a function of e^2, this time setting $f^2 = 0.01$. The dip around $e^2 \sim 0.01$ corresponds to the point where the error changes sign. This feature is also present on Fig. 6(b) that shows the error made by directly expanding the analytical formula of eq. (A23) in powers of e^2 and f^2. Decreasing the value of e^2 below the threshold $e^2 = f^2$ has no effect on the accuracy of the solution which becomes limited by the value of f^2, hence the saturation observed on the left side of both graphs. Above the threshold, one recovers the expected power laws in e^2 indicating the good numerical convergence properties of the method.

4 DISCUSSION

We have presented a new numerical method to compute the inviscid inertial modes of a rotating near-spherical container. This is based on the fully spectral discretization of the angular and radial directions using spherical harmonics in the angular directions and Chebyshev as well as Gegenbauer polynomials in the radial direction. We have shown how the method can be used to solve the Poincaré equation and the no penetration condition simultaneously as an algebraic polynomial eigenvalue problem and we have employed it to recover the inertial modes of a sphere and an oblate spheroid numerically with an accuracy limited by machine precision only (Sections 3.1 and 3.2). We have also shown how the method of equivalent spherical boundary introduced by Smith (1974) can be used to compute the inertial modes inside a boundary

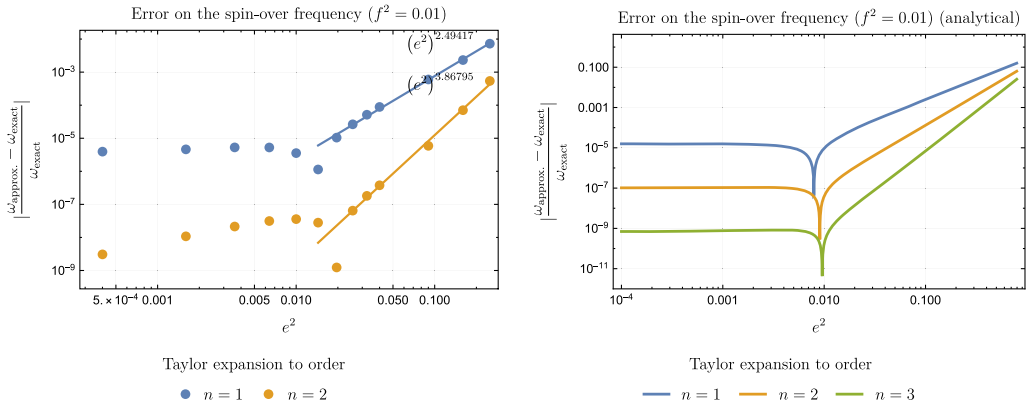

Figure 6. Triaxial ellipsoid—comparison of the eigenvalue of the spin-over mode computed using a Taylor expansion of the boundary condition with their analytical values as a function of the squared eccentricities e^2 and for $f^2 = 0.01$. The figure on the right-hand side shows the error resulting from the direct Taylor expansion of eq. (A23).

that deviates only slightly from a sphere. We substantiated this technique with an analysis of its numerical convergence for the inertial modes of lowest degree both in an oblate axisymmetric ellipsoid and a triaxial ellipsoid with small eccentricities (Sections 3.2 and 3.3).

The demonstration of the well posedness and numerical convergence of the method exposed in this paper in the context of inviscid inertial modes is an important first step towards its application to other problems for which there exists no analytical solution. It is not limited to the study of the sole Poincaré equation and can, in principle, be applied to the resolution of any system of differential equations in near-spherical geometry. Such problems are ubiquitous to the fields of planetology and geophysical/astrophysical fluid dynamics. Future foreseen applications include the study of the impact of inertial modes on the global rotation of a planet via coupling with the Liouville equation of rotational dynamics. This will be the subject of a future paper by the authors (Triana *et al.* 2018). This study also investigates the effect of viscosity. The effects of stratification and magnetization of the liquid core are also among possible applications. Such studies are natural extensions to the formalism of this paper via inclusion of the equations for heat diffusion and magnetic induction. With minor modifications, the spectral discretization described here can also accommodate multilayered physical configurations. This would allow to couple the dynamics of the liquid core to that of a viscoelastic and self-gravitating mantle with topography. These studies are long-term endeavours that are currently being investigated by the authors.

ACKNOWLEDGEMENTS

The authors would like to thank J. Vidal and N. Schaeffer for the useful discussions in the first stage of development of the method which lead to this paper. We would also like to thank S. Olver and the PETSc and SLEPc support teams for their help with technical details in the making of this work. The research leading to these results has received funding from the European Research Council (ERC) under the European Union's Horizon 2020 research and innovation programme (Advanced Grant agreement No. 670874).

REFERENCES

Aldridge, K.D. & Toomre, A., 1969. Axisymmetric inertial oscillations of a fluid in a rotating spherical container, *J. Fluid Mech.,* **37**(2), 307–323.

Backus, G. & Rieutord, M., 2017. Completeness of inertial modes of an incompressible inviscid fluid in a corotating ellipsoid, *Phys. Rev.,* **95**(5).

Balay, S., Gropp, W.D., McInnes, L.C. & Smith, B.F., 1997. Efficient management of parallelism in object oriented numerical software libraries, in *Modern Software Tools in Scientific Computing,* pp. 163–202, eds Arge, E., Bruaset, A.M. & Langtangen, H.P., Birkhäuser Press.

Balay, S. *et al.*, 2017a. PETSc users manual, Tech. Rep, ANL-95/11, Revision 3.8, Argonne National Laboratory.

Balay, S. *et al.*, 2017b. 'PETSc'. Available at: http://www.mcs.anl.gov/petsc, accessed online on 1 Nov 2018.

Bryan, G.H., 1889. The waves on a rotating liquid spheroid of finite ellipticity, *Phil. Trans. R. Soc. Lond., A,* **180,** 187–219.

Campos, C. & Roman, J.E., 2016. Parallel Krylov solvers for the polynomial eigenvalue problem in SLEPc, *SIAM J. Sci. Comput.,* **38**(5), S385–S411.

Cébron, D., Le Bars, M., Leontini, J., Maubert, P. & Le Gal, P., 2010. A systematic numerical study of the tidal instability in a rotating triaxial ellipsoid, *Phys. Earth Planet. Inter.,* **182**(1-2), 119–128.

Chan, K.H., Zhang, K. & Liao, X., 2010. An EBE finite element method for simulating nonlinear flows in rotating spheroidal cavities, *Int. J. Numer. Methods Fluids,* **63**(3), 395–414.

Greenspan, H.P., 1968. *The Theory of Rotating Fluids,* Cambridge Univ. Press.

Hernandez, V., Roman, J.E. & Vidal, V., 2005. SLEPc: a scalable and flexible toolkit for the solution of eigenvalue problems, *ACM Trans. Math. Softw.,* **31**(3), 351–362.

Hough, S.S., 1895. The oscillations of a rotating ellipsoidal shell containing fluid, *Phil. Trans. R. Soc. Lond., A,* **186,** 469–506.

Ivers, D., 2017a. Enumeration, orthogonality and completeness of the incompressible Coriolis modes in a tri-axial ellipsoid, *Geophys. Astrophys. Fluid Dyn.,* **111**(5), 333–354.

Ivers, D., 2017b. Tilted incompressible Coriolis modes in spheroids, *J. Fluid Mech.,* **833,** 131–163.

Kelley, D.H., Triana, S.A., Zimmerman, D.S., Tilgner, A. & Lathrop, D.P., 2007. Inertial waves driven by differential rotation in a planetary geometry, *Geophys. Astrophys. Fluid Dyn.,* **101**(5-6), 469–487.

Kudlick, M.D., 1966. *On transient motions in a contained, rotating fluid,* PhD thesis, Massachusetts Institute of Technology, Cambridge, MA.

Malkus, W., 1968. Precession of the Earth as the cause of geomagnetism: experiments lend support to the proposal that precessional torques drive the Earth's dynamo, *Science,* **160**(3825), 259–264.
Morize, C., Le Bars, M., Le Gal, P. & Tilgner, A., 2010. Experimental determination of zonal winds driven by tides, *Phys. Rev. Lett.,* **104**(21).
Morse, P. & Feshbach, H., 1953. *Methods of Theoretical Physics,* McGraw-Hill.
Olver, S. & Townsend, A., 2013. A fast and well-conditioned spectral method, *SIAM Rev.,* **55**(3), 462–489.
Poincaré, H., 1885. Sur l'équilibre d'une masse fluide animée d'un mouvement de rotation, *Acta Math.,* **7**(1), 259–380.
Rieutord, M., 2014. *Fluid Dynamics: An Introduction,* Springer International Publishing.
Rieutord, M. & Valdettaro, L., 1997. Inertial waves in a rotating spherical shell, *J. Fluid Mech.,* **341,** 77–99.
Rieutord, M., Georgeot, B. & Valdettaro, L., 2000. Inertial waves in a rotating spherical shell: attractors and asymptotic spectrum, *J. Fluid Mech.,* **435,** 103–144.
Schmitt, D., 2006. Numerical study of viscous modes in a rotating spheroid, *J. Fluid Mech.,* **567,** 399–414.
Schmitt, D. & Jault, D., 2004. Numerical study of a rotating fluid in a spheroidal container, *J. Comput. Phys.,* **197**(2), 671–685.
Smith, M.L., 1974. The scalar equations of infinitesimal elastic-gravitational motion for a rotating, slightly elliptical Earth, *Geophys. J. R. astr. Soc.,* **37**(3), 491–526.
Thomson, W., 1880. XXIV. Vibrations of a columnar vortex, *London Edinburgh Dublin Phil. Mag. J. Sci.,* **10**(61), 155–168.
Triana, S.A., Rekier, J., Trinh, A. & Dehant, V., 2018. The coupling between inertial and rotational eigenmodes in planets with liquid cores (under revision).
Vantieghem, S., 2014. Inertial modes in a rotating triaxial ellipsoid, *Proc. R. Soc., A,* **470,** doi:10.1098/rspa.2014.0093.
Vidal, J. & Schaeffer, N., 2015. Quasi-geostrophic modes in the Earth's fluid core with an outer stably stratified layer, *Geophys. J. Int.,* **202**(3), 2182–2193.
Zhang, K., Liao, X. & Earnshaw, P., 2004. On inertial waves and oscillations in a rapidly rotating spheroid, *J. Fluid Mech.,* **504,** 1–40.

APPENDIX A: ANALYTICAL SOLUTIONS

The idea is to introduce a new (frequency-dependent) set of coordinates $\{u, v, w\}$,

$$x = X(u, v, w) \tag{A1a}$$

$$y = Y(u, v, w) \tag{A1b}$$

$$z = \beta Z(u, v, w), \tag{A1c}$$

with the rescaling factor

$$\beta = \sqrt{\frac{1-\lambda^2}{\lambda^2}}, \qquad \text{where} \qquad \lambda = \frac{\omega}{2\Omega}, \tag{A2}$$

so as to turn the Poincaré equation (eq. 4) into a Laplace equation:

$$\nabla^2 p_0 - \frac{1}{\lambda^2}(\hat{\mathbf{z}}\cdot\nabla)^2 p_0 = \left(\frac{\partial^2 p_0}{\partial x^2}\right)_{y,z} + \left(\frac{\partial^2 p_0}{\partial y^2}\right)_{x,z} - \beta^2\left(\frac{\partial^2 p_0}{\partial z^2}\right)_{x,y} \tag{A3}$$

$$= \left(\frac{\partial^2 p_0}{\partial X^2}\right)_{Y,Z} + \left(\frac{\partial^2 p_0}{\partial Y^2}\right)_{X,Z} + \left(\frac{\partial^2 p_0}{\partial Z^2}\right)_{X,Y} \tag{A4}$$

$$= 0. \tag{A5}$$

The set of coordinates $\{u, v, w\}$ should be chosen so that the Laplace equation is separable and the no-penetration boundary condition (eq. 5) is easy to implement.

From the implicit expression for the general ellipsoid in $\mathbb{R}^3$

$$\Phi \equiv \frac{x^2}{a^2} + \frac{y^2}{b^2} + \frac{z^2}{c^2} - 1 = 0, \tag{A6}$$

the (unnormalized) normal vector $\mathbf{n} \sim \nabla\Phi$ at a surface point $x\hat{\mathbf{x}} + y\hat{\mathbf{y}} + z\hat{\mathbf{z}}$ writes

$$\mathbf{n} = \frac{x}{a^2}\hat{\mathbf{x}} + \frac{y}{b^2}\hat{\mathbf{y}} + \frac{z}{c^2}\hat{\mathbf{z}}. \tag{A7}$$

Therefore, the boundary condition (eq. 5) in Cartesian coordinates reads

$$-\left(\frac{\mathrm{i}y\lambda}{b^2} + \frac{x\lambda^2}{a^2}\right)\left(\frac{\partial p_0}{\partial x}\right)_{y,z} + \left(\frac{\mathrm{i}x\lambda}{a^2} - \frac{y\lambda^2}{b^2}\right)\left(\frac{\partial p_0}{\partial y}\right)_{x,z} + \left(\frac{z}{c^2} - \frac{z\lambda^2}{c^2}\right)\left(\frac{\partial p_0}{\partial z}\right)_{x,y} = 0. \tag{A8}$$

evaluated at a surface point $x\hat{\mathbf{x}}+y\hat{\mathbf{y}}+z\hat{\mathbf{z}}$. To rewrite the boundary condition (eq. A8) in terms of the new set of coordinates $\{u, v, w\}$, we compute the Jacobian of the transformation of coordinates

$$[\mathbf{J}]=\begin{bmatrix} \left(\frac{\partial X}{\partial u}\right)_{v,w} & \left(\frac{\partial X}{\partial v}\right)_{u,w} & \left(\frac{\partial X}{\partial w}\right)_{u,v} \\ \left(\frac{\partial Y}{\partial u}\right)_{v,w} & \left(\frac{\partial Y}{\partial v}\right)_{u,w} & \left(\frac{\partial Y}{\partial w}\right)_{u,v} \\ \beta\left(\frac{\partial Z}{\partial u}\right)_{v,w} & \beta\left(\frac{\partial Z}{\partial v}\right)_{u,w} & \beta\left(\frac{\partial Z}{\partial w}\right)_{u,v} \end{bmatrix} \tag{A9}$$

and deduce

$$\begin{bmatrix} \left(\frac{\partial p_0}{\partial x}\right)_{y,z} & \left(\frac{\partial p_0}{\partial y}\right)_{x,z} & \left(\frac{\partial p_0}{\partial z}\right)_{x,y} \end{bmatrix} = \begin{bmatrix} \left(\frac{\partial p_0}{\partial u}\right)_{v,w} & \left(\frac{\partial p_0}{\partial v}\right)_{u,w} & \left(\frac{\partial p_0}{\partial w}\right)_{u,v} \end{bmatrix} \cdot [\mathbf{J}]^{-1}. \tag{A10}$$

We now show that such a convenient set of coordinates can be found in spherical, spheroidal and ellipsoidal geometries. Note that in the sequel, we implicitly assume $0<|\lambda|<1$. Section 2.7 of Greenspan (1968) shows that all inertial modes in general bounded geometries have a half-frequency $-1\leq\lambda\leq 1$, that $\lambda=\pm 1$ is not an eigenfrequency, and that $\lambda=0$ is an eigenfrequency with infinite multiplicity.

A1 Sphere and oblate spheroid

The appropriate set of coordinates in this case is the (frequency-dependent) set of *bi-spheroidal* coordinates $\{\xi, \mu, \phi\}$[2], which are defined, in terms of the Cartesian coordinates, as

$$x = k\sqrt{1-\xi^2}\sqrt{1-\mu^2}\cos\phi, \tag{A11a}$$

$$y = k\sqrt{1-\xi^2}\sqrt{1-\mu^2}\sin\phi, \tag{A11b}$$

$$z = \beta k\xi\mu, \tag{A11c}$$

with β as previously (eq. A2) and

$$k=\sqrt{a^2+\frac{c^2}{\beta^2}}=a\sqrt{\frac{1-e^2\lambda^2}{1-\lambda^2}}, \tag{A12}$$

where $0<\xi<1$, $-\xi<\mu<\xi$ and $0<\phi<2\pi$. Note that these coordinates only map a bounded domain shaped as a pair of *cuberdons* joined along their base (corresponding to $\xi=\mu$). For convenience, we allow a double covering of this domain by extending μ to $-1<\mu<1$. Then, the level surfaces of ξ are (prolate or oblate) spheroids, those of μ are half-spheroids, and those of ϕ are vertical half-planes. Fig. A1 gives a graphical representation of these coordinates in the xz-plane. Note how this system of coordinates is *non-orthogonal*.

Under the above transformation, the Poincaré equation takes the form of a Laplace equation, of which the general solutions are solid bi-spheroidal harmonics,

$$p=\sum_{\ell=0}^{+\infty}\sum_{m=-\ell}^{+\ell} p_{\ell m}\mathrm{P}_\ell^m(\xi)\mathrm{P}_\ell^m(\mu)\mathrm{e}^{\mathrm{i}m\phi}, \tag{A13}$$

where the $p_{\ell m}$ are constants and P_ℓ^m is the degree-ℓ order-m associated Legendre function of the first kind. Regularity conditions prohibit the appearance of associated Legendre functions of the second kind Q_ℓ^m.

One interest of bi-spheroidal coordinates is that the surface of the oblate spheroid is a level surface of ξ,

$$\frac{x^2+y^2}{a^2}+\frac{z^2}{c^2}=1 \qquad \Leftarrow \qquad \xi=|\lambda|\sqrt{\frac{1-e^2}{1-e^2\lambda^2}}, \tag{A14}$$

which makes it easier to impose the no-penetration boundary condition. The latter requires the normal velocity to vanish, and can be expressed in terms of the pressure as eq. (A8), written in bi-spheroidal coordinates. Plug eq. (A13) into eq. (A8):

$$\sum_{\ell=0}^{+\infty}\sum_{m=-\ell}^{+\ell} p_{\ell m}\left((1-\lambda^2)\,\mathrm{sign}(\lambda)\mathrm{P}_\ell^{m\prime}\left(|\lambda|\sqrt{\frac{1-e^2}{1-e^2\lambda^2}}\right)-m\sqrt{(1-e^2)(1-e^2\lambda^2)}\mathrm{P}_\ell^m\left(|\lambda|\sqrt{\frac{1-e^2}{1-e^2\lambda^2}}\right)\right)\mathrm{P}_\ell^m(\mu)\mathrm{e}^{\mathrm{i}m\phi}=0. \tag{A15}$$

[2]Note that these are different from the orthogonal *oblate spheroidal coordinates* presented in Appendix C.

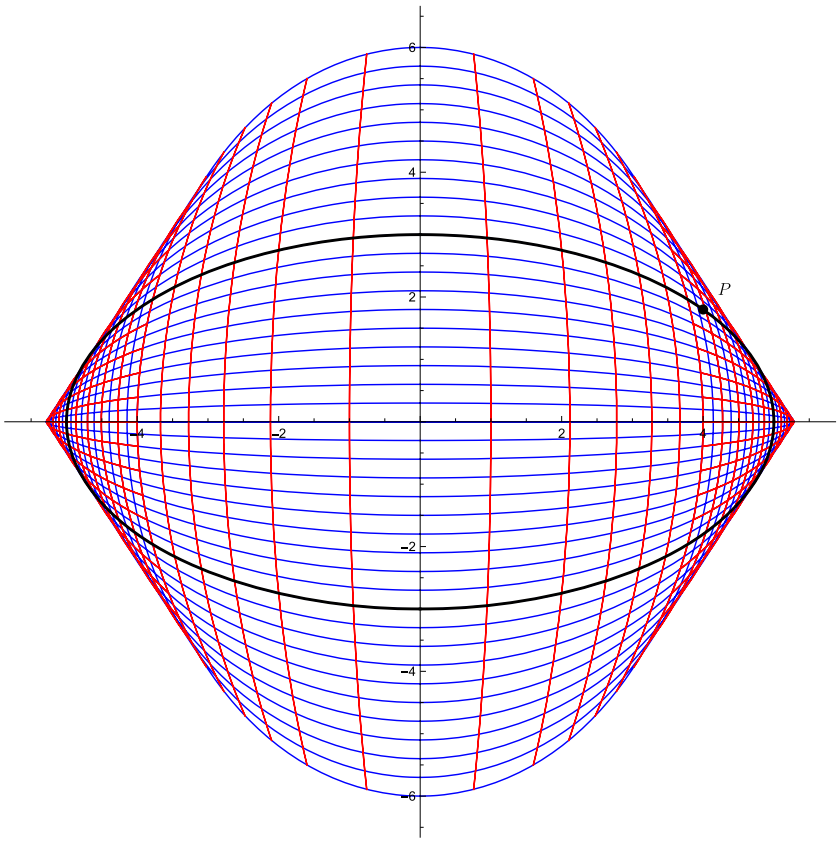

Figure A1. 2-D projection of the set of bi-spheroidal coordinates (eq. A11) for $\lambda = \frac{1}{2}$ in the xz-plane ($\phi = 0$). Blue curves are level surfaces of constant ξ and red curves are level surfaces of constant μ. The point P belongs to the physical ellipsoid that is shown as the thick black curve.

The functions $\mathrm{P}_\ell^m(\mu)\mathrm{e}^{\mathrm{i}m\phi}$ form a basis of surface spheroidal harmonics over the surface of the oblate spheroid. The boundary condition therefore leaves the coefficients $p_{\ell m}$ uncoupled, another advantage of bi-spheroidal coordinates. By orthogonality of the surface spheroidal harmonics, each harmonic coefficient has to vanish. The frequencies of the inertial modes in an oblate spheroid correspond to those values of λ or ω that allow non-zero values for $p_{\ell m}$, that is, one of the multiplicative factors vanishes. After some rearrangement,

$$\mathrm{P}_\ell^{m\prime}\left(\lambda\sqrt{\frac{1-e^2}{1-e^2\lambda^2}}\right) - \frac{m\sqrt{(1-e^2)(1-e^2\lambda^2)}}{1-\lambda^2}\mathrm{P}_\ell^m\left(\lambda\sqrt{\frac{1-e^2}{1-e^2\lambda^2}}\right) = 0. \tag{A16}$$

The sphere corresponds to the special case where $e^2 = 0$, in which case one recovers eq. (2.12.8) of Greenspan (1968).

The so-called *planetary modes* (Rieutord 2014) or *r-modes*, are a special family of solutions that satisfy $\ell = |m| + 1$. Inserting the latter into eq. (A16) reduces it to an equation of the first degree in λ with solution (Zhang *et al.* 2004),

$$\lambda = \frac{\mathrm{sign}(m)}{1 + |m|(1-e^2)}. \tag{A17}$$

The *spin-over mode* is the simplest member of this family, corresponding to $m = \pm 1$ and $\ell = 2$.

A2 Triaxial ellipsoid

The appropriate set of coordinates in this case is the (frequency-dependent) set of *bi-ellipsoidal* coordinates $\{\rho, \mu, \nu\}$, which are defined, in terms of the Cartesian coordinates, as

$$x = \pm\frac{\rho\mu\nu}{hk} \tag{A18a}$$

$$y = \pm\frac{\sqrt{\rho^2-h^2}\sqrt{\mu^2-h^2}\sqrt{h^2-\nu^2}}{h\sqrt{k^2-h^2}} \tag{A18b}$$

$$z = \pm\frac{\beta\sqrt{k^2-\rho^2}\sqrt{k^2-\mu^2}\sqrt{k^2-\nu^2}}{k\sqrt{k^2-h^2}}, \tag{A18c}$$

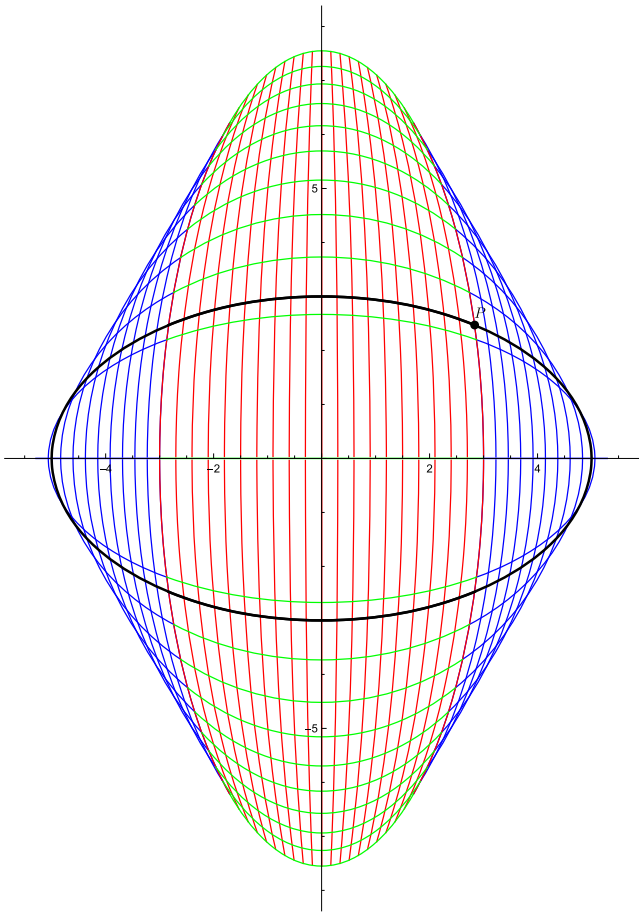

(A) xz-plane

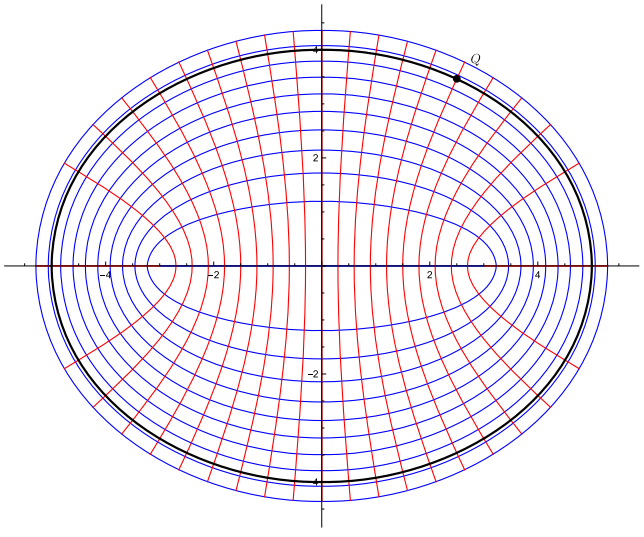

(B) xy-plane

Figure A2. 2-D projections of the set of bi-ellipsoidal coordinates (eq. A18) for $\lambda = \frac{1}{2}$ in the xz-plane (ν or $\mu = h$) and yz-plane (ν or $\mu = k$), respectively. Blue curves are level surfaces of constant μ, red curves are level surfaces of constant ν and green curves are level surfaces of constant ρ. The point P and Q belong to the physical ellipsoid that is shown as the thick black curve.

with β and k as previously (eqs A2–A12) and

$$h = \sqrt{a^2 - b^2} = a\sqrt{1 - f^2}, \tag{A19}$$

where $h < \rho < k$, $h < \mu < \rho$ and $0 < \nu < h$. Note that these coordinates only map one octant of a bounded domain shaped as a pair of cuberdons joined along their base (corresponding to $\rho = \mu$), hence the $\pm$ signs. For convenience, we allow a double covering of this domain by extending μ to $h < \mu < k$. Then, the level surfaces of ρ and μ are (sections of) ellipsoids, those of ν are (sections of) 1-sheeted hyperboloids. Fig. A2 gives a graphical representation of these coordinates in the *xz*- and *xy*-planes. Note how this system of coordinates is *non-orthogonal*.

Under the above transformation, the Poincaré equation takes the form of a Laplace equation, of which the general solutions are solid bi-ellipsoidal harmonics,

$$p = \sum_{n=0}^{\infty} \sum_{p=1}^{2n+1} c_{np} \mathrm{E}_{n,p}(\rho) \mathrm{E}_{n,p}(\mu) \mathrm{E}_{n,p}(\nu), \tag{A20}$$

where the c_{np} are constants and $\mathrm{E}_{n,p}$ is the degree-n index-p Lamé function of the first kind[3] (slightly modified to ensure that it always evaluates to a real number). Regularity conditions prohibit the appearance of Lamé functions of the second kind $\mathrm{F}_{n,p}$.

One interest of bi-ellipsoidal coordinates is that the surface of the triaxial ellipsoid is a level surface of ρ,

$$\frac{x^2}{a^2} + \frac{y^2}{b^2} + \frac{z^2}{c^2} = 1 \qquad \Leftarrow \qquad \rho = a, \tag{A21}$$

which makes it easier to impose the no-penetration boundary condition. The latter requires the normal velocity to vanish, and can be re-expressed in terms of the pressure as eq. (A8), written in bi-ellipsoidal coordinates. Plug eq. (A20) into eq. (A8):

$$\begin{aligned}
&\sum_{n=0}^{\infty} \sum_{p=1}^{2n+1} c_{np} \left(a(\mu^2 - \nu^2)\lambda \frac{\sqrt{(1-f^2)(1-e^2\lambda^2)(1-e^2\lambda^2 - f^2(1-\lambda^2))}}{\sqrt{(a^2 f^2 - \mu^2)(a^2 f^2 - \nu^2)}} \mathrm{E}'_{n,p}(a) \mathrm{E}_{n,p}(\mu) \mathrm{E}_{n,p}(\nu) \right. \\
&\left. + \mathrm{E}_{n,p}(a) \left(\nu \left(1 - e^2\lambda^2 - \frac{\mu^2 (1-\lambda^2)}{a^2} \right) \mathrm{E}'_{n,p}(\mu) \mathrm{E}_{n,p}(\nu) - \mu \left(1 - e^2\lambda^2 - \frac{\nu^2 (1-\lambda^2)}{a^2} \right) \mathrm{E}_{n,p}(\mu) \mathrm{E}'_{n,p}(\nu) \right) \right) = 0.
\end{aligned} \tag{A22}$$

The functions $\mathrm{E}_{n,p}(\mu)\mathrm{E}_{n,p}(\nu)$ form a basis of surface ellipsoidal harmonics over the surface of the triaxial ellipsoid. The boundary condition therefore only slightly couples the coefficients c_{np}, another advantage of bi-ellipsoidal coordinates. The second term of eq. (A22) only mixes terms of the same degree and symmetry. Indeed, the second-line terms can be rewritten as a sum of surface bi-ellipsoidal harmonics (Hough 1895). There is, however, no general expression and each degree and symmetry has to be considered individually. By orthogonality of the surface ellipsoidal harmonics, each harmonic coefficient has to vanish. This can be rewritten as a number of homogeneous matrix equations (one for each degree and symmetry) for the coefficients c_{np}. The frequencies of the inertial modes in a triaxial ellipsoid correspond to those values of λ or ω that allow non-zero values for c_{np}, that is, that cancel the determinant of the matrix.

We now list the half-frequency of the first few inertial modes in a triaxial ellipsoid.

For the spin-over mode (an equatorially antisymmetric mode of degree $n = 2$)

$$\lambda^2 = \frac{1 - f^2}{(2 - e^2)(2 - e^2 - f^2)}. \tag{A23}$$

The equatorially symmetric modes of degree 3 are

$$\lambda^2 = \frac{(1-f^2)\left(65 - 4e^2 - 63f^2 + 2e^2 f^2 + 12f^4 \pm \sqrt{4000 - 400e^2 - 7800f^2 + 600e^2 f^2 + 5321f^4 - 282e^2 f^4 - 1480f^6 + e^4 f^4 + 40e^2 f^6 + 144f^8}\right)}{(15 - 4e^2 - 4f^2 + e^2 f^2)(15 - 4e^2 - 22f^2 + 3e^2 f^2 + 8f^4)}. \tag{A24}$$

The equatorially antisymmetric modes of degree 3 are

$$\lambda^2 = \frac{(1 - f^2)\left(7 - 8e^2 - 3f^2 + 2e^4 + 2e^2 f^2 \pm (1 - e^2)\sqrt{4(1 - e^2)^2 + f^4}\right)}{(3 - 2e^2 - 2f^2 + e^2 f^2)(15 - 22e^2 - 4f^2 + 8e^4 + 3e^2 f^2)}. \tag{A25}$$

APPENDIX B: SPHERICAL HARMONICS DECOMPOSITIONS

We give the spherical harmonics coefficients of the expressions that appear in eqs (4) and (5) in spherical coordinates:[4]

$$\left(\nabla^2 \phi\right)_{\ell,m}(r) = \left(\frac{\mathrm{d}^2}{\mathrm{d}r^2} + \frac{2}{r}\frac{\mathrm{d}}{\mathrm{d}r} - \frac{\ell(\ell+1)}{r^2} \right) \phi_{\ell,m}(r), \tag{B1}$$

[3] see, for example, pp. 1304-1309 of Morse & Feshbach (1953) for reference.

[4] Those expressions depend on the choice of normalization. Here, we use the semi-normalized spherical harmonics for which one has $Y_0^0 = 1$.

$$\left(\frac{\mathrm{d}^2}{\mathrm{d}z^2}\phi\right)_{\ell,m}(r) = \frac{\sqrt{(\ell+1)^2-m^2}\sqrt{(\ell+2)^2-m^2}}{15+16\ell+4\ell^2}\left(\frac{\mathrm{d}^2}{\mathrm{d}r^2}+\frac{2\ell+5}{r}\frac{\mathrm{d}}{\mathrm{d}r}+\frac{\ell^2+4\ell+3}{r^2}\right)\phi_{\ell+2,m}(r)$$
$$+\frac{2\ell(\ell+1)-1-2m^2}{4\ell^2+4\ell-3}\left(\frac{\mathrm{d}^2}{\mathrm{d}r^2}+\frac{2}{r}\frac{\mathrm{d}}{\mathrm{d}r}-\frac{\ell(\ell+1)}{r^2}\right)\phi_{\ell,m}(r)$$
$$+\frac{\sqrt{(\ell-1)^2-m^2}\sqrt{\ell^2-m^2}}{4\ell^2-8\ell-3}\left(\frac{\mathrm{d}^2}{\mathrm{d}r^2}+\frac{3-2\ell}{r}\frac{\mathrm{d}}{\mathrm{d}r}+\frac{\ell(\ell-2)}{r^2}\right)\phi_{\ell-2,m}(r), \tag{B2}$$

$$\left((\hat{\mathbf{r}}\cdot\hat{\mathbf{z}})\frac{\mathrm{d}\phi}{\mathrm{d}z}\right)_{\ell,m}(r) =$$
$$\left(\frac{\sqrt{(\ell+1-m)(\ell+2-m)(\ell+m+1)(\ell+2+m)}}{4(\ell+2)^2-1}\frac{\mathrm{d}}{\mathrm{d}r}\right.$$
$$\left.+\frac{\sqrt{(\ell^2+5\ell+6)(\ell+3)(\ell+2-m)(\ell-m+1)(\ell+m+1)(\ell+2+m)}}{(2\ell+3)(2\ell+5)\sqrt{\ell+2}}\frac{1}{r}\right)\phi_{\ell+2,m}(r)$$
$$+\frac{1}{4\ell^2+4\ell-3}\left((-1+2\ell(\ell+1)-2m^2)\frac{\mathrm{d}}{\mathrm{d}r}+\frac{(\ell^2+\ell-3m^2)}{r}\right)\phi_{\ell,m}(r)$$
$$\left(\frac{\sqrt{(\ell-1-m)(\ell-m)(\ell+m-1)(\ell+m)}}{4\ell^2-8\ell-3}\frac{\mathrm{d}}{\mathrm{d}r}\right.$$
$$\left.+\frac{\sqrt{(\ell^2-3\ell+2)(\ell-2)(\ell-1-m)(\ell-m)(\ell+m-1)(\ell+m)}}{(4\ell^2-8\ell+3)\sqrt{\ell-1}}\frac{1}{r}\right)\phi_{\ell-2,m}(r), \tag{B3}$$

$$((\hat{\mathbf{z}}\times\hat{\mathbf{r}})\cdot\nabla\phi)_{\ell,m}(r) = \frac{2im}{r}\phi_{\ell,m}(r). \tag{B4}$$

APPENDIX C: OBLATE SPHEROIDAL COORDINATES

It is possible to extend the usage of spherical harmonics to the treatment of equations written in oblate spheroidal coordinates:

$$\begin{cases} x = c\sqrt{1+\xi^2}\sin\theta\cos\phi \\ y = c\sqrt{1+\xi^2}\sin\theta\sin\phi \\ z = c\xi\cos\theta. \end{cases} \tag{C1}$$

The level surfaces labelled with different constant values of ξ correspond to a family of confocal spheroids with foci separated by a distance $2c > 0$ in the xy-plane.

A scalar function given in oblate spheroidal coordinates can be expanded on a series of spherical harmonics just as easily as if it were given in spherical coordinates. The only difference being that, the coordinate θ no longer represents the polar angle (*geocentric* colatitude) but rather the angle between the basis vector $\hat{\theta}$ and the horizontal as illustrated on Fig. C1 (*geodetic* colatitude). The ξ coordinate now plays a role similar to that of the radial spherical coordinate r. In oblate spheroidal coordinates, the (truncated) expansion of the reduced pressure reads

$$p(\xi,\theta,\phi) = \sum_{\ell=0}^{L}\sum_{m=-\ell}^{\ell} p_{\ell,m}(\xi)Y_\ell^m(\theta,\phi). \tag{C2}$$

The trick to using spherical harmonics expansion effectively for the resolution of differential equations in these coordinates consists in realizing that the result of any differential operator acting on a single harmonic function, Y_ℓ^m, can be written as a finite sum of harmonic functions multiplied by some power of a *common pre-factor*:

$$\frac{1}{2(\xi^2+\cos^2\theta)}. \tag{C3}$$

When the equation to solve consists of the sum of differential operators, each with its own power of the pre-factor (eq. C3), the idea is to reduce the whole equation to the same denominator. This generates products of the spherical harmonics in each numerator with some power of $\cos^2\theta$ (which has a simple harmonic expansion in terms of Y_2^0 and Y_0^0 only). These products can be reduced to a finite sum over spherical harmonics using the usual rules. This technique critically reduces the coupling between each resulting ODE which would otherwise be infinite. In practice, we use the Mathematica package *TenGSHui* to expand the equations in oblate spheroidal harmonics.

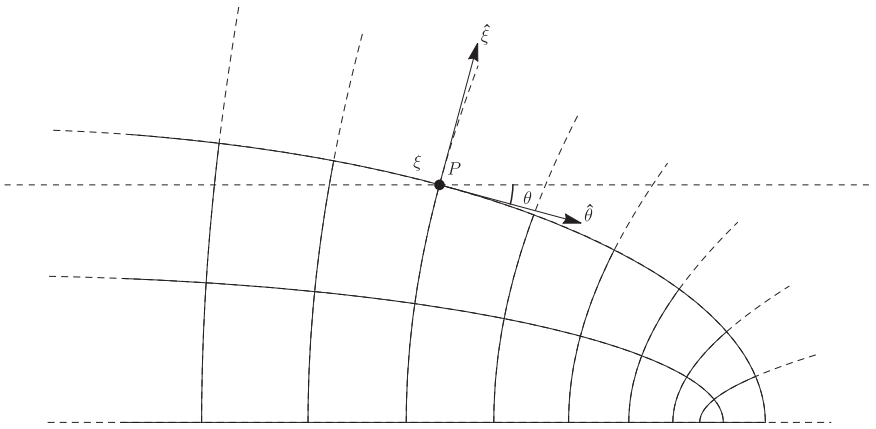

Figure C1. Localization of a point P by means of its oblate spheroidal coordinates (ξ, θ) at an arbitrary azimuthal angle ϕ. Level surfaces of constant ξ are oblate spheroids of linear eccentricity $c > 0$. The basis vector $\hat{\theta}$ makes an angle θ with the horizontal direction.

APPENDIX D: SERIES EXPANSION OF AN ELLIPSOID

The coefficients of the expansion of the triaxial ellipsoid surface in spherical harmonics which appear in eq. (14) are given below to second order in the squared eccentricities e^2 and f^2:

$$
\begin{aligned}
\epsilon_{0,0} &= -\frac{11e^4}{120} + \frac{e^2 f^2}{20} - \frac{e^2}{6} - \frac{11 f^4}{120} - \frac{f^2}{6} \\
\epsilon_{2,-2} &= -\frac{1}{28}\sqrt{\frac{3}{2}} e^2 f^2 + \frac{5 f^4}{28\sqrt{6}} + \frac{f^2}{2\sqrt{6}} \\
\epsilon_{2,0} &= -\frac{5e^4}{42} + \frac{e^2 f^2}{28} - \frac{e^2}{3} + \frac{5 f^4}{84} + \frac{f^2}{6} \\
\epsilon_{2,2} &= -\frac{1}{28}\sqrt{\frac{3}{2}} e^2 f^2 + \frac{5 f^4}{28\sqrt{6}} + \frac{f^2}{2\sqrt{6}} \\
\epsilon_{4,-4} &= \frac{3 f^4}{8\sqrt{70}} \\
\epsilon_{4,-2} &= \frac{3 f^4}{28\sqrt{10}} - \frac{3e^2 f^2}{14\sqrt{10}} \\
\epsilon_{4,0} &= \frac{3e^4}{35} - \frac{3e^2 f^2}{35} + \frac{9 f^4}{280} \\
\epsilon_{4,2} &= \frac{3 f^4}{28\sqrt{10}} - \frac{3e^2 f^2}{14\sqrt{10}} \\
\epsilon_{4,4} &= \frac{3 f^4}{8\sqrt{70}}.
\end{aligned}
\tag{D1}
$$